



Review

# Multiband Superconductivity, Polarons, Jahn-Teller Polarons, Heterogeneity, and High-Temperature Superconductivity

 Annette Bussmann-Holder <sup>1,\*</sup>  and Hugo Keller <sup>2</sup> 
<sup>1</sup> Max-Planck-Institute for Solid State Research, Heisenbergstr. 1, D-70569 Stuttgart, Germany

<sup>2</sup> Physik-Institute of the University of Zürich, University of Zürich, 8057 Zürich, Switzerland; keller@physik.uzh.ch

\* Correspondence: a.bussmann-holder@web.de or a.bussmann-holder@fkf.mpg.de

**Abstract:** Early on, oxides were ruled out from superconductivity, since they are typically large-band-gap insulators. Nevertheless, a rather small number of them were found to be superconducting, with transition temperatures up to 14 K and a remarkably low carrier density. This was the starting point of K. Alex Müller (KAM) becoming interested in superconductivity in oxides. Step by step, he advanced the research on oxides and finally discovered, together with J. Georg Bednorz, high-temperature superconductivity (HTSC) in the perovskite-type compound Ba-La-Cu-O. Even though he was inspired by specific and clear ideas in his search, he added new impact in the understanding of HTSC for many years after receipt of the Nobel prize for this discovery.

**Keywords:** perovskite oxides; Jahn-Teller effect; polarons; high-temperature cuprate superconductors

## 1. Introduction

The first oxide to exhibit superconductivity was discovered in 1964, namely reduced SrTiO<sub>3</sub> (STO), which becomes superconducting at  $T_c = 0.3$  K [1]. At that time, this was a remarkable observation, which caused novel theoretical interpretations well beyond BCS theory [2]. In particular, the soft transverse optic mode of STO was supposed to play a crucial role in the pairing mechanism. New interest in doped STO arose only recently when more attention was paid to the ultralow carrier density in this compound. Soon after STO superconductivity was reported in 1964 in the tungsten bronze Na<sub>x</sub>WO<sub>3</sub>, with  $T_c = 0.5$  K [3]. In 1973, LiTi<sub>2</sub>O<sub>4</sub> was discovered with  $T_c = 13.7$  K, followed by BaPb<sub>1-x</sub>Bi<sub>x</sub>O<sub>3</sub> in 1975 with  $T_c = 13$  K [4]. In 1980, Nb-doped SrTiO<sub>3</sub> with a maximum of  $T_c = 0.8$  K was observed, which is the first two-gap superconductor [5]. Like in the BaPb<sub>1-x</sub>Bi<sub>x</sub>O<sub>3</sub> system,  $T_c$  adopts a dome-like dependence on  $x$ , respectively Nb, now well known among the cuprate high-temperature superconductors (HTSs). What is remarkable about these oxides is the fact that the electron (hole) concentration is only  $n = 2 - 4 \times 10^{21} / \text{cm}^3$ . This is almost one order of magnitude smaller than in a normal (superconducting) metal. While this fact has long been overlooked, recently it has attracted a lot of attention, where many new interpretations have been offered [6].

Following, however, KAM's strategy, he concluded that if the density of states in these oxides is so low, then the pairing interaction must be extremely large in order to achieve the observed superconducting transition temperatures. In conventional weak coupling BCS theory, the formula for  $T_c$  is [7]:

$$T_c = 1.13 \Theta_D \exp\left[-\frac{1}{N(E_F) V^*}\right], \quad (1)$$

where  $N(E_F)$  is the electron concentration per elementary cell at the Fermi edge and  $V^*$  is the electron–electron interaction, which must be attractive to obtain superconductivity. Then, one notices that the product  $N(E_F) V^*$  must exhibit a certain order of magnitude to



**Citation:** Bussmann-Holder, A.; Keller, H. Multiband Superconductivity, Polarons, Jahn-Teller Polarons, Heterogeneity, and High-Temperature Superconductivity. *Condens. Matter* **2024**, *9*, 56. <https://doi.org/10.3390/condmat9040056>

Academic Editor: José Lorenzana

Received: 8 November 2024

Revised: 9 December 2024

Accepted: 12 December 2024

Published: 19 December 2024



**Copyright:** © 2024 by the authors. Licensee MDPI, Basel, Switzerland. This article is an open access article distributed under the terms and conditions of the Creative Commons Attribution (CC BY) license (<https://creativecommons.org/licenses/by/4.0/>).

obtain a finite transition temperature  $T_c$ . This requires for the oxides that if the electron concentration  $N(E_F)$  is small, the interaction  $V^*$  must be very strong to achieve these large values of  $T_c$ . This leads directly to the following question:

What is so special about oxides? Why do they have holes instead of electrons?

The oxygen ion and also the heavier chalcogenide ions in their doubly negatively charged state are peculiar as compared to almost all other ions, since they are unstable as free ions.

In simple oxides like MgO, CaO, and SrO, the oxygen ion polarizability  $\alpha(\text{O}^{2-})$  depends linearly on the volume  $V$  of the oxygen ion; in tetrahedrally coordinated oxides, this dependence is enhanced to a  $V^2$  dependence. In anisotropic configurations, as is realized in spinels and ferroelectric perovskite oxides  $\alpha \approx V^{3-4}$  [8]. In addition, it is a strong function of temperature and pressure. These properties are a consequence of the fact that the outer  $2p$ -electrons of  $\text{O}^{2-}$  tend to delocalize and hybridize with nearest neighbor transition metal  $d$ -states. The degree of hybridization can be triggered through the dynamics, thereby leading to a “dynamical covalency” [9]. The oxygen ion cannot be assigned to a fixed rigid ionic radius but instead space increments have to be introduced, which can be related to  $p-d$  hybridization degrees of freedom.

Quantum mechanical calculation of the oxygen ion polarizability within the Watson sphere model [10], where the free  $\text{O}^{2-}$  ion is surrounded by a homogeneously  $2+$  charged sphere, show that upon varying the radius  $R_W$  of this sphere, the oxygen ion polarizability can be obtained as a function of its volume (Figure 1) [11].

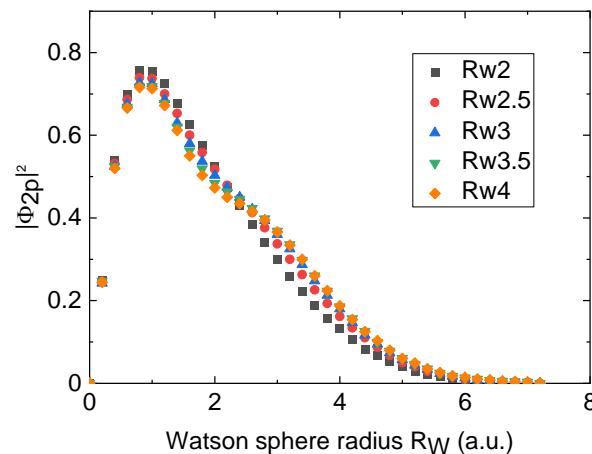


**Figure 1.** Oxygen ion  $\text{O}^{2-}$   $p$ -wave function  $|\Phi_{2p}|^2$  as a function of its radius as defined by the Watson sphere radius  $R_W$  (after Ref. [11]).

Apparently, the wave function does not shift rigidly with increasing  $R_W$ , but forms increments that tend to overlap with the coordinating transition metal ions. This is best exemplified by looking at the charge density difference (Figure 2), where charge is depleted in the intermediate regions.

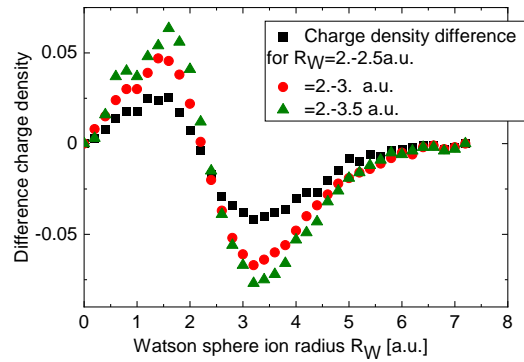


**Figure 2.** Difference in the oxygen ion charge density for various radii differences as given in the figure (after Ref. [12]).

The consequences of this unusual behavior are as follows:  $O^{1-}$  is a bound state;  $O^{2-}$  is resonant and unstable. Therefore, electron doping is impossible in oxides, and hole doping is the only possibility to dope oxides, thus leading to hole superconductivity [13]. Alternatives are that strong anharmonicity dominates oxides with tendencies to lattice and electronic instabilities. Besides of the above extraordinary role of the oxygen ion for hole-doped superconductivity, KAM was inspired by his friend Harry Thomas to consider Jahn-Teller (JT) ions to play another special role [14]. While primarily starting with nickelates, the missing success in the search for HTSC lead to cuprates [15]. By assuming an electron to be located at a certain lattice site, two of the ligands move in and the other two move out: the energy is lowered. The same is true for the reversed case and a second minimum appears. The energy gain is the Jahn-Teller stabilization energy  $E_{JT}$  (Figure 3).

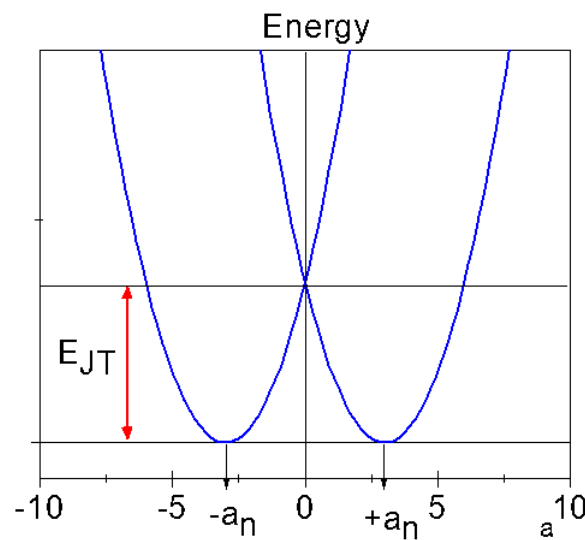


**Figure 3.** Ground state energy of the Jahn-Teller polaron with ionic displacements  $\pm a_n$ , where the energy gain  $E_{JT}$  as compared to the undistorted configuration is given by the red arrow (after Ref. [14]).

The ground-state energy for the Jahn-Teller polaron is then given by

$$E_k^{(0)} = E_0^{(0)} + \frac{\hbar^2 k^2}{2m_{\text{eff}}} \tag{2}$$

with the effective mass  $m_{\text{eff}}$  being enlarged as compared to the bare electronic mass. Limiting cases of this simplified model yield the relevant physics of the problem as outlined above, namely  $E_{\text{JT}} \ll t$ , where  $t$  is the hopping integral. The distortion due to the coupling to the electronic motion is small and is almost unaffected, i.e., free-electron-like. With increasing JT energy, the distortion increases, and for  $E_{\text{JT}} \gg t$  an isolated JT molecular complex results. The competition between localization and itineracy is thus an inherent property of the JT polaron problem. Combining both of the above, namely oxygen ion polarizability and instability and JT ions, limits the search for HTSC to rather few systems, namely nickelates and cuprates. In addition, for both of these oxide compounds, very much alike to ferroelectric-type perovskite oxides, it is known that it is almost impossible to grow them without any defects or in perfect stoichiometry. One of the prototypical perovskites, SrTiO<sub>3</sub> (STO), changes its properties completely upon replacing almost homoeopathic amounts of Sr with Ca. The same holds for introducing very small dopings of Nb. This implies that intrinsic heterogeneity governs the ground state character. Similarly, cuprate HTSCs are also non-homogeneous and superconductivity is only observed in a limited doping region. Typically, they are grown as ceramics and single crystals are difficult to achieve. This leads to the conclusion that perovskite oxides including cuprates are non-uniform and this structural diverseness is essential for their physical properties.

## 2. Isotope Effects

For BCS-type superconductors, the prediction of an isotope effect on  $T_c$  is a hallmark to highlight the role of electron–phonon coupling. With a few exceptions, an isotope effect has always been observed in conventional superconductors. That is why also cuprate HTSCs have been readily tested for the isotope effect. The first oxygen (<sup>16</sup>O/<sup>18</sup>O) isotope effect (OIE) experiments were carried out on Ba<sub>2</sub>YCu<sub>3</sub>O<sub>7</sub> and Ba<sub>2</sub>EuCu<sub>3</sub>O<sub>7</sub> samples at optimum doping and only a very tiny OIE on  $T_c$  ( $\Delta T_c/T_c < 0.2\%$ ) was found [16]. The conclusions from this experiment were drawn almost immediately after this report, namely that the missing effects must be interpreted in terms of a novel pairing mechanism beyond electron–phonon interaction. Since the undoped parent compounds of cuprate HTSCs are all antiferromagnets (AFMs), the proximity between HTSC and antiferromagnetism was taken as evidence that magnetic fluctuations are the origin for the hole pairing in cuprates (see, e.g., Ref. [17]). Even though a number of further isotope experiments at various doping levels were carried out subsequently, where isotope effects were observed [18–20], the first results [16] dominated the scene. However, a breakthrough result was achieved by the Stuttgart [21] and Zurich [22,23] groups almost simultaneously, when they concentrated on the question which oxygen ions in optimally doped YBa<sub>2</sub>Cu<sub>3</sub>O<sub>x</sub> (YBCO) systems are responsible for the OIE [site-selective oxygen isotope effect (SOIE)]. In the structure of YBCO, there are three different oxygen lattice positions: plane (p), apex (a), and chain (c). The Zurich group applied a two-step oxygen exchange process in order to prepare partially substituted <sup>16</sup>O/<sup>18</sup>O YBa<sub>2</sub>Cu<sub>3</sub>O<sub>6+x</sub> samples required for SOIE investigations [23]. As a result, quite opposite to expectations, namely that the apex oxygen ions (a) should exhibit the largest OIE [22], the (p) oxygen ions were mainly responsible for the total OIE [23]. In order to demonstrate that this finding also holds in the underdoped region, additional SOIE studies were performed for Y<sub>1-x</sub>Pr<sub>x</sub>Ba<sub>2</sub>Cu<sub>3</sub>O<sub>7-δ</sub> ( $x = 0, 0.3, 0.4$ ) [24,25], and the results are summarized in (Figure 4). It is obvious from the figure that at all doping levels the main contribution to the total OIE arises from the (p) oxygen ions.

This was verified in various experiments, but also through a rather unconventional strategy, where the OIE on the magnetic penetration depth  $\lambda$  (superfluid density  $\propto \lambda^{-2}$ ) was investigated using various experimental techniques [magnetization, magnetic torque, and muon spin rotation ( $\mu$ SR)] [26]. As an example of such a study, the results of the OIE on the in-plane superfluid density observed for single-crystal La<sub>2-x</sub>Sr<sub>x</sub>CuO<sub>4</sub> using magnetic torque is depicted in Figure 5 [27], where a pronounced doping-dependent OIE on the in-plane superfluid density [ $\propto \lambda_{ab}^{-2}(0)$ ] is evident.

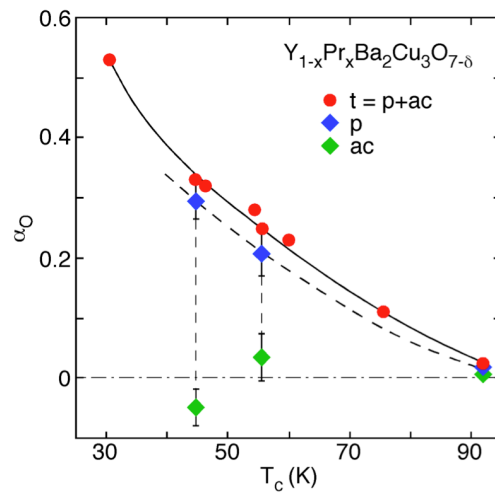


**Figure 4.** The OIE coefficients  $\alpha_O^t$  (red circles),  $\alpha_O^p$  (blue diamonds), and  $\alpha_O^{ac}$  (green diamonds) as a function of  $T_c$  for  $Y_{1-x}Pr_xBa_2Cu_3O_{7-\delta}$  ( $t$  = total: all oxygen sites;  $p$ : planar oxygen sites;  $ac$ : apex and chain oxygen sites). All lines are guides to the eye (after Ref. [26]).

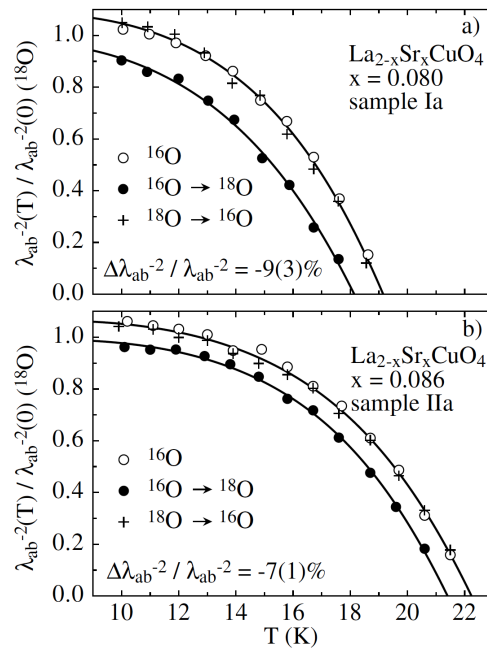


**Figure 5.** Temperature dependence of the in-plane superfluid density  $\lambda_{ab}^{-2}(T)/\lambda_{ab}^{-2}(0)$  for single-crystal  $La_{2-x}Sr_xCuO_4$  extracted from magnetic torque measurements: (a)  $x = 0.080$ ; (b)  $x = 0.086$ . For more details see [27] (from Ref. [27]).

Even though within BCS theory no OIE on the penetrations depth (superfluid density) is expected, these experiments were carried out under the assumption that a bi-polaronic mechanism would support an OIE on the penetration depth (superfluid density), with a site-specific result. This was indeed observed in an SOIE study of the in-plane magnetic penetration depth  $\lambda_{ab}$  in  $Y_{0.6}Pr_{0.4}Ba_2Cu_3O_{7-\delta}$  by means of  $\mu$ SR [25]. Consistent with the SOIE on  $T_c$  (see Figure 4), the one on  $\lambda_{ab}$  was largest also for oxygen atoms in the  $CuO_2$  planes ( $p$ ), whereas the one on the ( $ac$ ) lattice positions was present, but much smaller. These unexpected and amazing results demonstrate clearly that two different structural components of the cuprate HTS systems play different roles in the respective physics, supporting the viewpoint of two order parameters and heterogeneity as essential ingredients, which will be addressed in more detail below.

### 3. Essential Ingredients for High-Temperature Superconductivity: Heterogeneities and Mixed Order Parameters in Cuprate Superconductors

Clear experimental evidence for intrinsic heterogeneity in the cuprates has been given by extended X-ray absorption fine structure (EXAFS) spectroscopy and pair distribution function analysis, where a stripe-like ordering has been detected [28]. Charge-rich areas and the fully symmetric undistorted charge-poor regions have been observed. Very intriguing demonstrations of their existence have been provided by the group of A. Bianconi, where clear correlations between oxygen-rich regions and charge density wave (CDW) puddles have been detected [29].

Opposite to a *s*-wave BCS superconductor and the conclusions obtained from the OIE experiments, the missing OIE at optimum doping readily led to the assumption that cuprate HTSs are governed by a single *d*-wave order parameter. This was supported by in-plane phase-coherent tunneling experiments (see, e.g., Refs. [30–32]) and a number of other experimental studies. In contrast, Sun et al. [33] performed a tunneling experiment along the *c*-axis of optimally doped YBa<sub>2</sub>Cu<sub>3</sub>O<sub>7-δ</sub> (YBCO), which is consistent with a pure *s*-wave order parameter. Furthermore, in a nuclear magnetic resonance (NMR) experiment, the temperature dependence of the NMR spin relaxation time  $T_2$  in different YBCO compounds was investigated [34]. The experimental results lie in between the theoretical calculations for a *s*- and a *d*-wave superconductor [35]; however, they are closer to the *d*-wave one. Based on these and other experimental findings, as well as theoretical considerations, KAM proposed that cuprate superconductors must have a mixed *s* + *d*-wave order parameter that reflects the intrinsic inhomogeneities (hole-rich and hole-poor stripe-like regions) in these systems [36–38].

In order to test the proposed concept of KAM, we performed detailed muon spin rotation ( $\mu$ SR) experiments.  $\mu$ SR is extremely sensitive in detecting any kind of local and global magnetic signatures in magnetic systems, including superconductors. In particular,  $\mu$ SR is a powerful tool to explore the pairing symmetry (*s*, *d*, and *s* + *d*) of a cuprate HTS in the *bulk* of a single-crystal sample. This is exemplified by measuring the temperature dependence of the magnetic penetration depths  $\lambda_a$ ,  $\lambda_b$ , and  $\lambda_c$  along the principal crystallographic axes *a*, *b*, and *c*. The University of Zurich group has conducted such studies on three different cuprate HTSs, revealing consistent and generic results [39–41].

As an example, the results of such a  $\mu$ SR study for single-crystal YBa<sub>2</sub>Cu<sub>3</sub>O<sub>7-δ</sub> are displayed in Figure 6, where the temperature dependences of the  $\mu$ SR relaxation rates  $\sigma_a \propto \lambda_a^{-2}$ ,  $\sigma_b \propto \lambda_b^{-2}$ , and  $\sigma_c \propto \lambda_c^{-2}$  are plotted [40]. Note that  $\sigma_a(T) \propto \lambda_a^{-2}(T)$  as well as  $\sigma_b(T) \propto \lambda_b^{-2}(T)$  exhibit a characteristic “up-turn” at low temperature. This is the signature of a coupled *s* + *d*-wave order parameter in the CuO<sub>2</sub> plane with a dominant *d*-wave order parameter ( $\approx 75\%$ ) and a small *s*-wave contribution ( $\approx 25\%$ ) [40,42]. However,  $\sigma_c(T) \propto \lambda_c^{-2}(T)$  is in accordance with a pure *s*-wave order parameter.

This experiment not only highlights the capabilities of  $\mu$ SR but it also provides clear evidence of the coexistence of two order parameters in cuprate HTSs, with major contributions of the *d*-wave order parameter in the *a*- and *b*-direction, whereas along the *c*-direction the *s*-wave order parameter is realized, in agreement with the *c*-axis tunneling results [33] mentioned above.

Of course, other experiments have also confirmed the intrinsic heterogeneity of cuprate HTSs and the two-component character of the condensate. Only few examples are given here: As already mentioned above, early on after performing the first NMR experiments Bulut and Scalapino [35] analyzed them in terms of a purely electronic model based on spin fluctuations and concluded that a *d*-wave only approach was unable to reproduce the experimental data. Some years later, it was shown that by using a mixed *s* + *d*-wave order parameter a very satisfactory description of the experiments could be achieved [43]. Furthermore, scanning tunneling microscope (STM) spectroscopy demonstrated that the electron tunneling process is essentially incoherent. These observations are favored by the *s*-wave pairing mechanism. However, the conductance curves were found to be substantially smeared in comparison with the conventional excitation spectra predicted in

BCS (isotropic *s*-wave) superconductors, suggesting the anisotropy of the gap functions in cuprate HTSs [44]. NMR experiments were able to disclose that the observed NMR shifts stem from two components and are in support of intrinsic heterogeneity [45,46]. Studies of the nonlinear conductivity in cuprate HTSs identified that intrinsic and universal superconducting gap inhomogeneity is highly relevant to understanding the superconducting properties of the cuprates [47]. Theoretically, a similar conclusion for the coexistence of *s* + *d*-wave superconductivity was reached by using a quantum Monte Carlo approach [48]. Another ansatz was based on the slave boson approach for a two-band model, where again coexistence regions of *s* + *d* channels were considered [49]. Of course, a number of related models exist, but this is beyond the scope of the article.

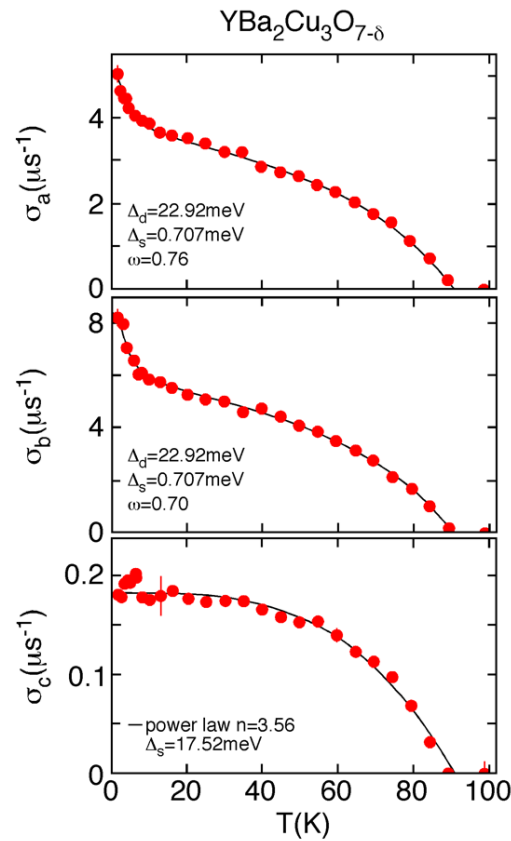


**Figure 6.** The  $\mu$ SR relaxation rates (superfluid densities)  $\sigma_a \propto \lambda_a^{-2}$ ,  $\sigma_b \propto \lambda_b^{-2}$ , and  $\sigma_c \propto \lambda_c^{-2}$  as a function of temperature measured along the three crystallographic directions *a*, *b*, and *c* (from top to bottom) for single-crystal  $\text{YBa}_2\text{Cu}_3\text{O}_{7-\delta}$ . In the figures, the extracted gap values  $\Delta_{d,s}$  are given together with their respective weights  $\omega$ . For  $\sigma_c(T)$ , a power law fit was used corresponding to a BCS-type temperature dependence (after Ref. [40]).

#### 4. Theoretical Understanding

The simplest and most transparent model for understanding the above findings is provided by a two-band model, where one band has mainly an *s*-electron character, whereas the second one constitutes the *d*-electron states. Interactions between both types of carriers are the important ingredient for two-band superconductivity. The Hamiltonian *H* reads as follows [50]:

$$H = H_0 + H_1 + H_2 + H_{12} \tag{3}$$



with

$$H_0 = \sum_{k_1, \sigma} \xi_{k_1} c_{k_1 \sigma}^+ c_{k_1 \sigma} + \sum_{k_2, \sigma} \xi_{k_2} d_{k_2 \sigma}^+ d_{k_2 \sigma} \quad (4)$$

$$H_1 = - \sum_{k_1, k'_1, q} V_1(k_1, k'_1) c_{k_1+q/2\uparrow}^+ c_{-k_1+q/2\downarrow}^+ c_{-k'_1+q/2\downarrow} c_{k'_1+q/2\uparrow} \quad (5)$$

$$H_2 = - \sum_{k_2, k'_2, q} V_2(k_2, k'_2) d_{k_2+q/2\uparrow}^+ d_{-k_2+q/2\downarrow}^+ d_{-k'_2+q/2\downarrow} d_{k'_2+q/2\uparrow} \quad (6)$$

$$H_{12} = - \sum_{k_1, k_2, q} V_{12}(k_1, k_2) [c_{k_1+q/2\uparrow}^+ c_{-k_1+q/2\downarrow}^+ d_{-k_2+q/2\downarrow} d_{k_2+q/2\uparrow} + h.c.] \quad (7)$$

where  $c^+$ ,  $c$ ,  $d^+$ , and  $d$  are electron creation and annihilation operators with spin  $\sigma$  and momentum  $k$ .  $H_0$  is the kinetic energy with hopping integrals  $\xi$  and  $V_i$  ( $i = 1, 2$ ) are the intraband pairing interactions. The term  $V_{12}$  represents the interband pairing interaction, where electrons are pairwise exchanged between the two bands. The pairing potentials  $V_i(k_i, k'_i)$  are assumed to be represented in a factorized form like  $V_i(k_i, k'_i) = V_i(\varphi_{k_i}, \psi_{k'_i})$ , where  $\varphi_{k_i}$ ,  $\psi_{k'_i}$  are cubic harmonics for anisotropic pairing, which yields for dimension  $D = 2$  and on-site pairing  $\varphi_{k_i} = 1$ ,  $\psi_{k'_i} = 1$ ; extended  $s$ -wave:  $\varphi_{k_i} = \cos k_x a + \cos k_y b = \gamma_{k_i}$ ; and  $d$ -wave:  $\varphi_{k_i} = \cos k_x a - \cos k_y b = \eta_{k_i}$ , where  $a$ ,  $b$  are the lattice constants along the  $x$ ,  $y$  directions. By performing a mean-field analysis of Equations (4)–(7), these transform to

$$H_{\text{red}} = \sum_{k_1, \sigma} \xi_{k_1} c_{k_1 \sigma}^+ c_{k_1 \sigma} + \sum_{k_2, \sigma} \xi_{k_2} d_{k_2 \sigma}^+ d_{k_2 \sigma} + \bar{H}_1 + \bar{H}_2 + \bar{H}_{12} \quad (8)$$

$$\begin{aligned} \bar{H}_i = & - \sum_{k'_i} [\Delta_{k'_i} c_{k'_i \uparrow}^+ c_{-k'_i \downarrow}^+ + \Delta_{-k'_i}^* c_{-k'_i \downarrow} c_{k'_i \uparrow}] \\ & + \sum_{k_i, k'_i} V_i(k_i, k'_i) \langle c_{k_i \uparrow}^+ c_{-k_i \downarrow}^+ \rangle \langle c_{-k'_i \downarrow} c_{k'_i \uparrow} \rangle \end{aligned} \quad (9)$$

$$\begin{aligned} \bar{H}_{12} = & \sum_{k_1, k_2} [V_{12}(k_1, k_2) \langle c_{k_1 \uparrow}^+ c_{-k_1 \downarrow}^+ \rangle d_{-k_2 \downarrow} d_{k_2 \uparrow} + V_{12}(k_1, k_2) \langle d_{-k_2 \downarrow} d_{k_2 \uparrow} \rangle c_{k_1 \uparrow}^+ c_{-k_1 \downarrow}^+ \\ & + V_{12}^*(k_1, k_2) d_{k_2 \uparrow}^+ d_{-k_2 \downarrow}^+ \langle c_{-k_1 \downarrow} c_{k_1 \uparrow} \rangle + V_{12}^*(k_1, k_2) c_{-k_1 \downarrow} c_{k_1 \uparrow} \langle d_{k_2 \uparrow}^+ d_{-k_2 \downarrow}^+ \rangle \\ & - V_{12}(k_1, k_2) \langle c_{-k_1 \downarrow} c_{k_1 \uparrow} \rangle \langle d_{-k_2 \downarrow} d_{k_2 \uparrow} \rangle - V_{12}^*(k_1, k_2) \langle c_{-k_1 \downarrow} c_{k_1 \uparrow} \rangle \langle d_{-k_2 \downarrow} d_{k_2 \uparrow} \rangle] \end{aligned} \quad (10)$$

where for  $i = 2$   $c$  is replaced by  $d$ .  $\xi_{k_i} = \varepsilon_i + \varepsilon_{k_i} - \mu$ , where  $\mu$  is the chemical potential. Furthermore, it is assumed that  $\langle c_{k_1+q/2\uparrow}^+ c_{-k_1+q/2\downarrow}^+ \rangle = \langle c_{k_1 \uparrow}^+ c_{-k_1 \downarrow}^+ \rangle \delta_{q,0}$ , and similarly for the  $d$  operators. Additionally, the following definitions are introduced:  $\Delta_{k'_i}^* = \sum_{k_i} V_i(k_i, k'_i) \langle c_{k_i \uparrow}^+ c_{-k_i \downarrow}^+ \rangle$  together with

$$\begin{aligned} B_{k_2}^* &= \sum_{k_2} V_{12}(k_1, k_2) \langle d_{k_2 \uparrow}^+ d_{-k_2 \downarrow}^+ \rangle, \\ A_{k_1}^* &= \sum_{k_2} V_{12}(k_1, k_2) \langle c_{k_2 \uparrow}^+ c_{-k_2 \downarrow}^+ \rangle, \end{aligned} \quad (11)$$

and  $V_{12}^* = V_{12}$ . The gap equations are self-consistently derived and are given by

$$\langle c_{k_1 \uparrow}^+ c_{-k_1 \downarrow}^+ \rangle = \frac{\bar{\Delta}_{k_1}^*}{2E_{k_1}} \tanh \frac{\beta E_{k_1}}{2} = \bar{\Delta}_{k_1}^* \Phi_{k_1} \quad (12)$$

$$\langle d_{k_2 \uparrow}^+ d_{-k_2 \downarrow}^+ \rangle = \frac{\bar{\Delta}_{k_2}^*}{2E_{k_2}} \tanh \frac{\beta E_{k_2}}{2} = \bar{\Delta}_{k_2}^* \Phi_{k_2} \quad (13)$$



with  $E_{k_2}^2 = \tilde{\epsilon}_{k_2}^2 + |\bar{\Delta}_{k_2}|^2$ ,  $\bar{\Delta}_{k_2} = \Delta_{k_2} + B_{k_2}$  and  $E_{k_1}^2 = \tilde{\epsilon}_{k_1}^2 + |\bar{\Delta}_{k_1}|^2$ ,  $\bar{\Delta}_{k_1} = \Delta_{k_1} + A_{k_1}$ , which results in the following self-consistent set of coupled equations:

$$\bar{\Delta}_{k_1} = \sum_{k'_1} V_1(k_1, k'_1) \bar{\Delta}_{k'_1} \Phi_{k'_1} + \sum_{k_2} V_{12}(k_1, k_2) \bar{\Delta}_{k_2} \Phi_{k_2} \quad (14)$$

$$\bar{\Delta}_{k_2} = \sum_{k'_2} V_2(k_2, k'_2) \bar{\Delta}_{k'_2} \Phi_{k'_2} + \sum_{k_1} V_{21}(k_1, k_2) \bar{\Delta}_{k_1} \Phi_{k_1} \quad (15)$$

Numerical solutions of the above equations yield the dependence of the gaps as a function of the chemical potential (Figure 7), i.e., doping and the interband interaction term  $V_{12}$ . If the interactions  $V$  are constants, the resulting gaps are momentum-independent. A more interesting case is obtained by assuming the following general momentum dependence of the intraband interactions  $V_i = g_\gamma^{(i)} + g_\gamma^{(i)} \gamma_k \gamma_{k'} + g_\eta^{(i)} \eta_k \eta_{k'}$  where, as pointed out above, the first term yields on-site pairing, the second extended  $s$ -wave pairing, and the last  $d$ -wave pairing. In the actual calculations,  $V_1$  is proportional to  $g_0$  while  $V_2$  is determined by either  $g_0$  or  $g_\eta$ . The two bands that are considered here are one-dimensional in the  $c$ -channel and two-dimensional in the  $d$ -channel with dispersion  $\epsilon_{k_2} = -2t_2(\cos k_x a + \cos k_y b)$ , where  $t_2$  corresponds to the second-nearest hopping. Later on, also the nearest neighbor  $t_1$  and interplanar  $t_4$  hopping are considered. The intraband interactions are chosen to be small such that both bands separately do not show superconductivity:  $V_1 = V_2 = 0.01$ , where  $V_1 = \tilde{V}_1 N_c$ ,  $V_2 = \tilde{V}_2 N_d$ . The self-consistent set of equations is solved numerically as a function of  $V_{12} = \tilde{V}_{12} \sqrt{N_c N_d}$ , where  $N_c$ ,  $N_d$  are the density of states in the  $c$ ,  $d$  band. The dome-like dependence of the coupled gaps reproduces very well the in the cuprate HTSs observed dependence on  $T_c$  as a function of doping. In addition, the figure clarifies that  $V_{12}$  plays a central role in the magnitude of  $T_c$  and the gaps, which increase nonlinearly with  $V_{12}$ . In all cases, the  $d$ -wave gap (squares) is the dominant one, whereas the  $s$ -wave gap (circles) is almost 60% smaller than the  $d$ -gap.

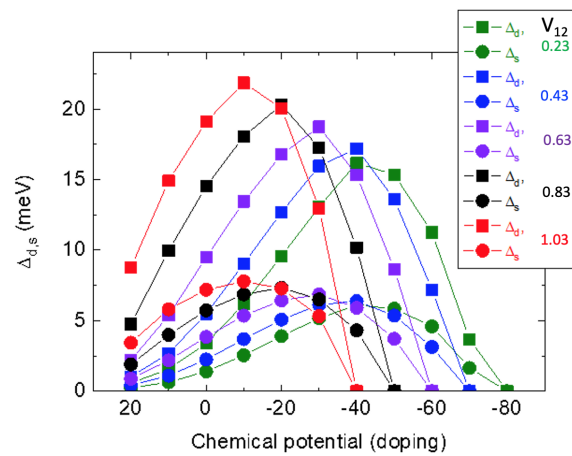


**Figure 7.** Dependence of the coupled gaps  $\Delta_{s,d}$  on the chemical potential for different coupling constants  $V_{12} = 0.23, 0.43, 0.63, 0.83, 1.03$  as indicated in the figure (after Ref. [50]).

In order to bring these results into contact with experimental data, the average gap values have been plotted as functions of  $T_c$  and compared to data for  $Y_{1-x}Ca_xBa_2Cu_3O_{7-\delta}$  in Figure 8 [51].

Apparently, good agreement between experiment and theory is given when taking two bands with inter- and intraband interactions into account. A special effect of using this approach is the fact that  $T_c$  can be significantly enhanced by the interband coupling term, even if the intraband couplings exhibit rather moderate values (Figure 9).

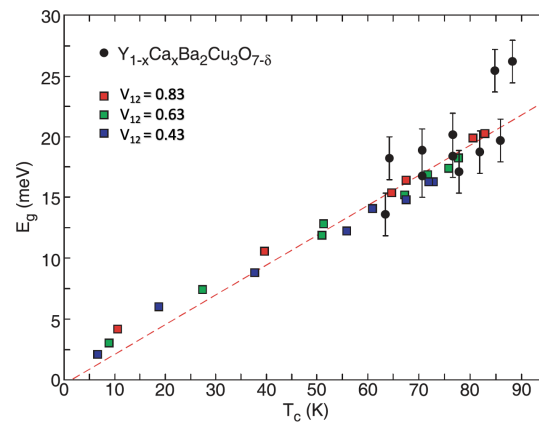


**Figure 8.** Dependence of the average gap value  $E_g$  as a function of  $T_c$ . The red, green, and blue square symbols stem from calculations for different values of  $V_{12}$ , as indicated in the figure. The black circles with bars are experimental data points for  $Y_{1-x}Ca_xBa_2Cu_3O_{7-\delta}$  (after Ref. [51]).

It was highlighted early on in the papers by Suhl, Matthias, and Walker [52] and Moskalenko [53] that, even independent of the sign of the interband coupling, enhancements of  $T_c$  as compared to single-band approaches a la BCS occur. As can be seen in Figure 9b, even in the case of both intraband interactions being too small to induce superconductivity, moderate values of  $V_{12}$  of the order of 0.5 lead to superconductivity at  $T_c \simeq 50$  K for mixed-symmetry  $s + d$  order parameters and  $T_c \simeq 28$  K for  $s + s$  symmetry order parameters.

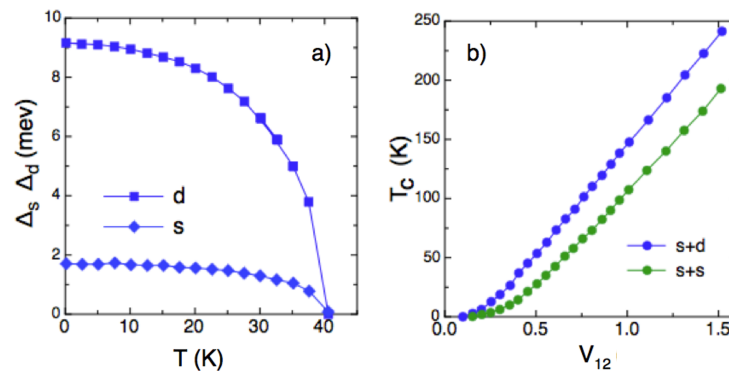


**Figure 9.** (a) Self-consistently derived coupled gaps  $\Delta_s$  and  $\Delta_d$  as a function of temperature  $T$  for interband coupling  $V_{12} = 0.4$ . (b)  $T_c$  as a function of  $V_{12}$  (average density of states of d- and s-band) for coupled gaps  $s + d$  (blue) and  $s + s$  (green) (after Ref. [50]).

## 5. Isotope Effects in a Multiband Polaron Approach

Polaron formation takes place if the coupling between the electrons (holes) and the lattice is neither too strong nor too weak, as has been outlined above. The mediate strength coupling between holes (electrons) and lattice vibrations (displacements) has two coupled and inseparable consequences, namely, the hole (electron) kinetic energy is slowed down, since it carries a lattice cloud, and the lattice energy is shifted, caused by the hole (electron) drag. One without the other is not possible. The easiest ansatz is here the Lang–Firsov approximation [54], which takes both renormalizations simultaneously into account. For the renormalized electron creation and annihilation operators, this yields the following [54]:

$$\tilde{c}_{\sigma i}^+ = c_{\sigma i}^+ \exp(\gamma_i \tilde{p}_i), \quad \tilde{c}_{\sigma i} = c_{\sigma i} \exp(-\gamma_i \tilde{p}_i) \quad (16)$$

where  $\tilde{p}_i$  is the normalized crystal momentum. For the lattice Hamiltonian, the following renormalizations hold [54]:

$$\tilde{H} = \sum_{q,j} \hbar \tilde{\omega}_{q,j} (\tilde{b}_{q,j}^+ \tilde{b}_{q,j} + 1/2) \tag{17}$$

with

$$\tilde{b}_q^+ = b_q^+ + \sum_q \gamma_i(q) c_i^+ c_i, \quad \tilde{b}_q = b_q + \sum_q \gamma_i(q) c_i^+ c_i, \tag{18}$$

and

$$\tilde{\omega}_{q,j}^2 = \omega_{q,j}^2 - \frac{\gamma_{q,j}^2}{N(E_F)} \sum_k \frac{1}{\varepsilon(k)} \tanh \frac{\varepsilon(k)}{k_B T} \tag{19}$$

with

$$\varepsilon(k) = -2t_1 [\cos(k_x a) + \cos(k_y b)] + 4t_2 \cos(k_x a) \cos(k_y b) \mp t_4 [\cos(k_x a) - \cos(k_y b)]^2 - \mu, \tag{20}$$

and  $\gamma$  being the dimensionless electron–phonon coupling as defined in Ref. [54]. The nearest  $t_1$  and second-nearest neighbor  $t_2$  and interplanar  $t_4$  hopping integrals are modified through the interaction with the lattice. Within this approach, an isotope effect on  $T_c$  may arise from either one of the hopping integrals, or from different combinations of them. Interestingly, the OIE on  $T_c$  stemming from  $t_1$  yields the wrong trend, whereas the combined action of  $t_2$  and  $t_4$  follows the experimental data (see Figure 10).

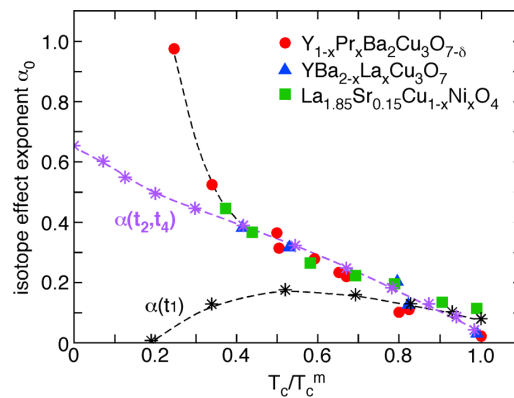


**Figure 10.** OIE exponent  $\alpha_O$  for various families of cuprate HTSs as a function of  $T_c/T_c^m$ , where  $T_c^m$  corresponds to the maximum  $T_c$  in a given family of cuprates. The red, blue, and green symbols are measured values for  $\alpha_O$  for the given families, as indicated in the figure. The dashed black line is a guide to the eye, and the dashed violet line and symbols show the calculated isotope effect stemming from the renormalization of  $t_2, t_4$  [ $\alpha(t_2, t_4)$ ], where the black dashed line and the black stars refer to the one related to  $t_1$  [ $\alpha(t_1)$ ] (from Ref. [55]).

This result allows to draw conclusions on the involved lattice displacements, namely those where oxygen atoms displacing towards the neighboring Cu ions are irrelevant (Figure 11, left), whereas a Jahn-Teller-type mode (Figure 11, right) supports the observed OIE (see Figure 10) when combined with a c-axis displacement. It is important to emphasize that not only the ionic displacements are affected by the polaronic distortion, but also the Cu spins. This issue has been addressed in detail in Ref. [56].

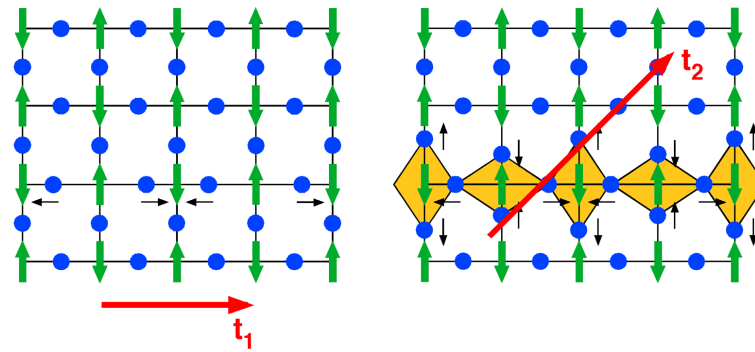


**Figure 11.** The copper–oxygen plane, where green arrows refer to the Cu ions whereas blue circles stand for the oxygen ions. **(left panel)** The displacement pattern of the oxygen ions related to the electronic hopping integral  $t_1$ . **(right panel)** The displacement pattern of the oxygen ions related to the electronic hopping integral  $t_2$ . The one involving  $t_4$ , which is relevant to describe the OIE on  $T_c$  (see Figure 10), is not shown, since it is out-of-plane (from Ref. [55]).

Briefly, the lattice response [Equations (18)–(20)] is also mentioned, which shows some unconventional signatures caused by the polaronic coupling (Figure 12). This is best exemplified through the Debye–Waller factor, which at high temperatures  $T$  appears to be conventional, i.e., decreasing steadily with decreasing  $T$ . However, around the so-called stripe temperature  $T^*$  a rapid increase sets in, signaling polaron coherence followed by a sudden drop near  $T_c$  and another increase below  $T_c$ . The drop at  $T_c$  is a consequence of the zero line nodes of the  $d$ -wave component of the order parameter, whereas the following increase stems from the  $s$ -wave component. This finding supports the two-component character and the coexistence of an  $s$ -wave and a  $d$ -wave order parameter. Upon inspecting the structure of a cuprate HTS, a possible assignment of them can be made in terms of the antiferromagnetic spin alignment in the planes and an out-of-plane almost ferroelectric-type polar component (see Figure 13).

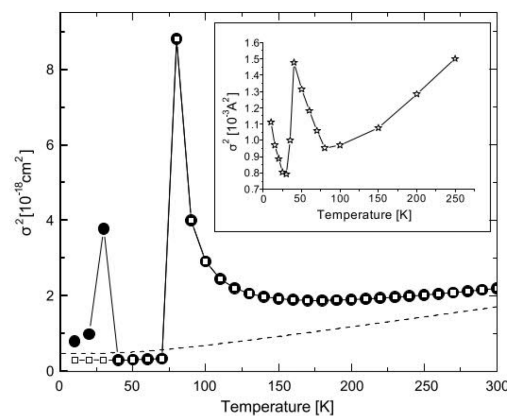


**Figure 12.** The calculated temperature dependence of the mean-square displacement  $\sigma^2$  (Debye–Waller factor) of the relative Cu–O displacement squared in the presence of the renormalized electronic hopping integrals  $t_2$  and  $t_4$  (full line and circles). The open circles refer to  $T > T_c$ , the full ones to  $T < T_c$ . The dashed line is the result for the case that polaronic effects are not involved. In the inset, experimental EXAFS data for  $\text{La}_{1.85}\text{Sr}_{0.15}\text{CuO}_4$  [57] are shown (from Ref. [58]).

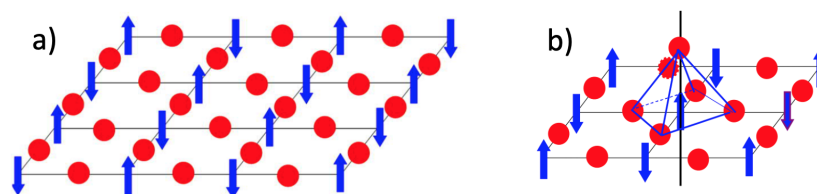


**Figure 13.** (a) In-plane antiferromagnet spin component. (b) Out-of-plane ferroelectric component. Both are uncoupled in the underdoped case.

## 6. Conclusions and Outlook for Further Search for High-Temperature Superconductivity

A reasonable undertaking to discover novel superconductors would be to look at transition metal oxides or chalcogenides, where the metal ion should be a JT-active one with a tendency to valence instability, thus ensuring that the ground state is intrinsically heterogeneous. In combination with the unconventional large polarizability of oxygen, chalcogen ions, respectively, fluctuating charge transfer is enabled, “dynamical covalency”, which enhances the charge–lattice coupling locally and allows for unusual lattice anomalies in conjunction with possible pairing instabilities. The electron–lattice interaction is not the conventional BCS electron–phonon interaction, which is long-range, but a local one outside the Born–Oppenheimer approximation. This leads to unconventional isotope effects, which are typically overlooked or even ignored in purely electronic or spin-fluctuation-based pairing scenarios. Furthermore, combined order parameters are a consequence that not only leads to agreement with puzzling experiments, but also accounts for the complexity in the electronic structure of cuprates, often avoided in strongly simplified alternative procedures. As pairing glue, we have identified (bi-) polaron formation, the starting point for the discovery of high-temperature superconductivity.

**Author Contributions:** Both authors (A.B.-H. and H.K.) have contributed equally to this work. All authors have read and agreed to the published version of the manuscript.

**Funding:** This research received no external funding.

**Data Availability Statement:** The data presented in this study are available upon reasonable request from the corresponding author.

**Acknowledgments:** We acknowledge very gratefully the support and many fruitful and highlighting discussions with K.A. Müller for many years.

**Conflicts of Interest:** The authors declare no conflicts of interest.

## References

1. Schooley, J.F.; Hosler, W.R.; Cohen, M.L. Superconductivity in Semiconducting SrTiO<sub>3</sub>. *Phys. Rev. Lett.* **1964**, *12*, 474–475. [[CrossRef](#)]
2. Appel, J. Soft-Mode Superconductivity in SrTiO<sub>3-x</sub>. *Phys. Rev.* **1969**, *180*, 508–516. [[CrossRef](#)]
3. Raub, C.J.; Sweedler, A.R.; Jensen, M.A.; Broadston, S.; Matthias, B.T. Superconductivity of Sodium Tungsten Bronzes. *Phys. Rev. Lett.* **1964**, *13*, 746–747. [[CrossRef](#)]
4. Sleight, A.W.; Gillson, J.L.; Bierstedt, P.E. High-temperature superconductivity in the BaPb<sub>1-x</sub>Bi<sub>x</sub>O<sub>3</sub> systems. *Solid State Commun.* **1975**, *17*, 27–28. [[CrossRef](#)]
5. Binnig, G.; Baratoff, A.; Hoenig, H.E.; Bednorz, J.G. Two-band superconductivity in Nb-doped SrTiO<sub>3</sub>. *Phys. Rev. Lett.* **1980**, *45*, 1352–1355. [[CrossRef](#)]
6. Gastiasoro, M.N.; Ruhman, J.; Fernandes, R.M. Superconductivity in dilute SrTiO<sub>3</sub>: A review. *Ann. Phys.* **2020**, *417*, 168107. [[CrossRef](#)]
7. Bardeen, J.; Cooper, L.N.; Schrieffer, J.R. Theory of Superconductivity. *Phys. Rev. B* **1957**, *108*, 1175–1204. [[CrossRef](#)]
8. Tessman, J.R.; Kahn, A.H.; Shockley, W. Electronic Polarizabilities of Ions in Crystals. *Phys. Rev.* **1953**, *92*, 890–895. [[CrossRef](#)]
9. Bilz, H.; Buttner, H.; Bussmann-Holder, A.; Vogl, P. Phonon anomalies in ferroelectrics and superconductors. *Ferroelectrics* **1987**, *73*, 493–500. [[CrossRef](#)]
10. Watson, R.E. Analytic Hartree-Fock Solutions for O<sup>2-</sup>. *Phys. Rev.* **1958**, *111*, 1108–1110. [[CrossRef](#)]
11. Bussmann, A.; Bilz, H.; Roenspiess, R.; Schwarz, K. Oxygen polarizability in ferroelectric phase transitions. *Ferroelectrics* **1980**, *25*, 343–346. [[CrossRef](#)]

12. Busmann-Holder, A. The polarizability model for ferroelectricity in perovskite oxides. *J. Phys. Condens. Matter* **2012**, *24*, 273202. [[CrossRef](#)] [[PubMed](#)]
13. Hirsch, J.E. *Superconductivity Begins with H*; World Scientific: Hackensack, NJ, USA; London, UK; Singapore, 2020.
14. Höck, K.-H.; Nickisch, H.; Thomas, H. Jahn-Teller effect in itinerant electron systems: The Jahn-Teller polaron. *Helv. Phys. Acta* **1983**, *56*, 237–243.
15. Bednorz, J.G.; Müller, K.A. Possible High  $T_c$  Superconductivity in the Ba-La-Cu-O System. *Z. Phys. B-Condens. Matter* **1986**, *64*, 189–193. [[CrossRef](#)]
16. Batlogg, B.; Cava, R.J.; Jayaraman, A.; van Dover, R.B.; Kourouklis, G.A.; Sunshine, S.; Murphy, D.W.; Rupp, L.W.; Chen, H.S.; White, A.; et al. Isotope Effect in the High- $T_c$  Superconductors  $\text{Ba}_2\text{YCu}_3\text{O}_7$  and  $\text{Ba}_2\text{EuCu}_3\text{O}_7$ . *Phys. Rev. Lett.* **1987**, *58*, 2333–2336. [[CrossRef](#)]
17. Moriya, T.; Takahashi, Y.; Ueda, K. Antiferromagnetic Spin Fluctuations and Superconductivity in Two-Dimensional Metals—A Possible Model for High  $T_c$  Oxides. *J. Phys. Soc. Jpn.* **1990**, *59*, 2905–2915. [[CrossRef](#)]
18. Crawford, M.K.; Farneth, W.E.; McCarron, E.M.; Harlow, R.L.; Moudren, A.H. Oxygen Isotope Effect and Structural Phase Transitions in  $\text{La}_2\text{CuO}_4$ -Based Superconductors. *Science* **1990**, *250*, 1390–1394. [[CrossRef](#)]
19. Franck, J.P.; Jung, J.; Mohamed, A.K.; Gyax, S.; Sproule, G.I. Observation of an oxygen isotope effect in superconducting  $(\text{Y}_{1-x}\text{Pr}_x)\text{Ba}_2\text{Cu}_3\text{O}_{7-\delta}$ . *Phys. Rev. B* **1991**, *44*, 5318–5321. [[CrossRef](#)]
20. Franck, J.P. Experimental studies of the isotope effect in high temperature superconductors. In *Physical Properties of High Temperature Superconductors IV*; Ginsberg, D.M., Ed.; World Scientific: Singapore, 1994; pp. 189–293.
21. Cardona, M.; Liu, R.; Thomsen, C.; Kress, W.; Schönherr, E.; Bauer, M.; Genzel, L.; König, W. Effect of isotopic substitution of oxygen on  $T_c$  and the phonon frequencies of high  $T_c$  superconductors. *Solid State Commun.* **1988**, *76*, 789–793. [[CrossRef](#)]
22. Müller, K.A. On the oxygen isotope effect and apex anharmonicity in high- $T_c$  cuprates. *Z. Phys. B-Condens. Matter* **1990**, *80*, 193–201. [[CrossRef](#)]
23. Zech, D.; Keller, H.; Conder, K.; Kaldis, E.; Liarokapis, E.; Poulakis, N.; Müller, K.A. Site-selective oxygen isotope effect in optimally doped  $\text{YBa}_2\text{Cu}_3\text{O}_{6+x}$ . *Nature* **1994**, *371*, 681–683. [[CrossRef](#)]
24. Zhao, G.M.; Ager, J.W., III; Morris, D.E. Site dependence of large oxygen isotope effect in  $\text{Y}_{0.7}\text{Pr}_{0.3}\text{Ba}_2\text{Cu}_3\text{O}_{6.97}$ . *Phys. Rev. B* **1996**, *54*, 14982–14985. [[CrossRef](#)]
25. Khasanov, R.; Shengelaya, A.; Morenzoni, E.; Angst, M.; Conder, K.; Savić, I.M.; Lampakis, D.; Liarokapis, E.; Tatsi, A.; Keller, H. Site-selective oxygen isotope effect on the magnetic field penetration depth in underdoped  $\text{Y}_{0.6}\text{Pr}_{0.4}\text{Ba}_2\text{Cu}_3\text{O}_{7-\delta}$ . *Phys. Rev. B* **2003**, *68*, 220506. [[CrossRef](#)]
26. Keller, H. Unconventional Isotope Effects in Cuprate Superconductors. In *Superconductivity in Complex Systems*; Müller, K.A., Busmann-Holder, A., Eds.; Structure and Bonding 114; Springer: Berlin/Heidelberg, Germany; New York, NY, USA, 2005; pp. 143–169.
27. Hofer, J.; Conder, K.; Sasagawa, T.; Zhao, G.M.; Willemin, M.; Keller, H.; Kishio, K. Oxygen-isotope effect on the in-plane penetration depth in underdoped  $\text{La}_{2-x}\text{Sr}_x\text{CuO}_4$  single crystals. *Phys. Rev. Lett.* **2000**, *84*, 4192–4195. [[CrossRef](#)] [[PubMed](#)]
28. Bianconi, A.; Saini, N.L.; Lanzara, A.; Missori, M.; Rossetti, T.; Oyanagi, H.; Yamaguchi, H.; Oka, K.; Ito, T. Determination of the Local Lattice Distortions in the  $\text{CuO}_2$  Plane of  $\text{La}_{1.85}\text{Sr}_{0.15}\text{CuO}_4$ . *Phys. Rev. Lett.* **1996**, *76*, 3412–3415. [[CrossRef](#)]
29. Campi, G.; Bianconi, A.; Poccia, N.; Bianconi, G.; Barba, L.; Arrighetti, G.; Innocenti, D.; Karpinski, J.; Zhigadlo, N.D.; Kazakov, S.M.; et al. Inhomogeneity of charge-density-wave order and quenched disorder in a high- $T_c$  superconductor. *Nature* **2015**, *525*, 359–362. [[CrossRef](#)] [[PubMed](#)]
30. Wollman, D.A.; Van Harlingen, D.J.; Lee, W.C.; Ginsberg, D.M.; Leggett, A.J. Experimental determination of the superconducting pairing state in YBCO from the phase coherence of YBCO-Pb dc SQUIDS. *Phys. Rev. Lett.* **1993**, *71*, 2134–2137. [[CrossRef](#)] [[PubMed](#)]
31. Tsuei, C.C.; Kirtley, J.R.; Chi, C.C.; Yu-Jahnes, Lock See; Gupta, A.; Shaw, T.; Sun, J.Z.; Ketchen, M.B. Pairing Symmetry and Flux Quantization in a Tricrystal Superconducting Ring of  $\text{YBa}_2\text{Cu}_3\text{O}_{7-\delta}$ . *Phys. Rev. Lett.* **1994**, *73*, 593–596. [[CrossRef](#)]
32. Brawner, D.A.; Ott, H.R. Evidence for an unconventional superconducting order parameter in  $\text{YBa}_2\text{Cu}_3\text{O}_{6.9}$ . *Phys. Rev. B* **1994**, *50*, 6530–6533. [[CrossRef](#)] [[PubMed](#)]
33. Sun, A.G.; Gajewski, D.A.; Maple, M.B.; Dynes, R.C. Observation of Josephson pair tunneling between a high- $T_c$  cuprate ( $\text{YBa}_2\text{Cu}_3\text{O}_{7-\delta}$ ) and a conventional superconductor (Pb). *Phys. Rev. Lett.* **1994**, *72*, 2267–2270. [[CrossRef](#)] [[PubMed](#)]
34. Stern, R.; Mali, M.; Roos, J.; Brinkmann, D. Spin pseudogap and interplane coupling in  $\text{Y}_2\text{Ba}_4\text{Cu}_7\text{O}_{15}$ : A  $^{63}\text{Cu}$  nuclear spin-spin relaxation study. *Phys. Rev. B* **1995**, *51*, 15478–15483. [[CrossRef](#)]
35. Bulut, N.; Scalapino, D.J. Calculation of the transverse nuclear relaxation rate for  $\text{YBa}_2\text{Cu}_3\text{O}_7$  in the superconducting state. *Phys. Rev. Lett.* **1991**, *67*, 2898–2901. [[CrossRef](#)] [[PubMed](#)]
36. Müller, K.A. Possible coexistence of  $s$ - and  $d$ -wave condensates in copper oxide superconductors. *Nature* **1995**, *377*, 133–135. [[CrossRef](#)]
37. Müller, K.A.; Keller, H.  $s$  and  $d$  Wave Symmetry Components in High-Temperature Cuprate Superconductors. In *High- $T_c$  Superconductivity 1996: Ten Years after the Discovery*; Kaldis, E., Liarokapis, E., Müller, K.A., Eds.; Kluwer Academic Publishers: Dordrecht, The Netherlands, 1997; pp. 7–29.
38. Müller, K.A. On the macroscopic  $s$ - and  $d$ -wave symmetry in cuprate superconductors. *Phil. Mag. Lett.* **2002**, *82*, 279–288. [[CrossRef](#)]



39. Khasanov, R.; Shengelaya, A.; Maisuradze, A.; La Mattina, F.; Bussmann-Holder, A.; Keller, H.; Müller, K.A. Experimental evidence for two gaps in the high-temperature  $\text{La}_{1.83}\text{Sr}_{0.17}\text{CuO}_4$  superconductor. *Phys. Rev. Lett.* **2007**, *98*, 057007. [[CrossRef](#)]
40. Khasanov, R.; Strässle, S.; Di Castro, D.; Masui, T.; Miyasaka, S.; Tajima, S.; Bussmann-Holder, A.; Keller, H. Multiple gap symmetries for the order parameter of cuprate superconductors from penetration depth measurements. *Phys. Rev. Lett.* **2007**, *99*, 237601. [[CrossRef](#)]
41. Khasanov, R.; Shengelaya, A.; Karpinski, J.; Bussmann-Holder, A.; Keller, H.; Müller, K.A.  $s$ -wave symmetry along the  $c$ -axis and  $s + d$  in-plane superconductivity in bulk  $\text{YBa}_2\text{Cu}_4\text{O}_8$ . *J. Supercond. Nov. Magn.* **2008**, *21*, 81–85. [[CrossRef](#)]
42. Bussmann-Holder, A.; Khasanov, R.; Shengelaya, A.; Maisuradze, A.; La Mattina, F.; Keller, H.; Müller, K.A. Mixed order parameter symmetries in cuprate superconductors. *Europhys. Lett.* **2007**, *77*, 27002. [[CrossRef](#)]
43. Bussmann-Holder, A. Evidence for  $s + d$  Wave Pairing in Copper Oxide Superconductors from an Analysis of NMR and NQR Data. *J. Supercond. Nov. Magn.* **2012**, *25*, 155–157. [[CrossRef](#)]
44. Hasegawa, T.; Nantoh, M.; Heike, S.; Takagi, S.; Ogino, M.; Kawasaki, M.; Koinuma, H.; Kitazawa, K. Scanning tunneling spectroscopy on high  $T_c$  superconductors. *J. Phys. Chem. Solids* **1993**, *54*, 1351–1357. [[CrossRef](#)]
45. Haase, J.; Slichter, C.P.; Williams, G.V.M. Evidence for two electronic components in high-temperature superconductivity from NMR. *J. Phys. Condens. Matter* **2009**, *21*, 455702. [[CrossRef](#)]
46. Bandur, D.; Nachtigal, J.; Lee, A.; Tsankov, S.; Haase, J. Cuprate universal electronic spin response and the pseudogap from NMR. *arXiv* **2024**, arXiv:2309.11874v3.
47. Pelc, D.; Vučković, M.; Grbić, M.S.; Požek, M.; Yu, G.; Sasagawa, T.; Greven, M.; Barišić, N. Emergence of superconductivity in the cuprates via a universal percolation process. *Nat. Commun.* **2018**, *9*, 4327. [[CrossRef](#)]
48. Li, Q.P.; Koltenbah, B.E.C.; Joynt, Robert. Mixed  $s$ -wave and  $d$ -wave superconductivity in high- $T_c$  systems. *Phys. Rev. B* **1993**, *48*, 437–455. [[CrossRef](#)]
49. Reyes, D.; Continentino, M.A.; Thomas, C.; Lacroix, C.  $s$ - and  $d$ -wave superconductivity in a two-band model. *Ann. Phys.* **2016**, *373*, 257–272. [[CrossRef](#)]
50. Micnas, R.; Robaszkiewicz, S.; Bussmann-Holder, A. Two-Component Scenarios for Non-Conventional (Exotic) Superconductors. In *Superconductivity in Complex Systems*; Müller, K.A., Bussmann-Holder, A., Eds.; Structure and Bonding 114; Springer: Berlin/Heidelberg, Germany, 2005; pp. 13–69.
51. Bussmann-Holder, A.; Keller, H. Polaron formation as origin of unconventional isotope effects in cuprate superconductors. *Eur. Phys. J. B* **2005**, *44*, 487–490. [[CrossRef](#)]
52. Suhl, H.; Matthias, B.T.; Walker, L.R. Bardeen-Cooper-Schrieffer Theory of Superconductivity in the Case of Overlapping Bands. *Phys. Rev. Lett.* **1959**, *3*, 552–555. [[CrossRef](#)]
53. Moskalenko, V. Superconductivity in metals with overlapping energy bands. *Fiz. Met. Metalloved.* **1959**, *8*, 2518–2529.
54. Lang, I.G.; Firsov, Y.A. Kinetic Theory of Semiconductors with Low Mobility. *Sov. Phys. JETP* **1962**, *16*, 1301–1318.
55. Keller, H.; Bussmann-Holder, A.; Müller, K.A. Jahn-Teller physics and high- $T_c$  superconductivity. *Mater. Today* **2008**, *11*, 38–46. [[CrossRef](#)]
56. Deng, H.-Y.; Lam, C.H.; Huang, H. A two-plaquette polaron picture for the single-hole state of cuprates. *Supercond. Sci. Technol.* **2012**, *25*, 075003. [[CrossRef](#)]
57. Oyanagi, H.; Zhang, C.; Tsukada, A.; Naito, M. Lattice instability in high temperature superconducting cuprates probed by X-ray absorption. *J. Phys. Conf. Ser.* **2008**, *108*, 012038. [[CrossRef](#)]
58. Bussmann-Holder, A.; Keller, H.; Bishop, A.R.; Simon, A.; Müller, K.A. Polaron coherence as origin of the pseudogap phase in high temperature superconducting cuprates. *J. Supercond. Nov. Magn.* **2008**, *21*, 353–357. [[CrossRef](#)]

**Disclaimer/Publisher’s Note:** The statements, opinions and data contained in all publications are solely those of the individual author(s) and contributor(s) and not of MDPI and/or the editor(s). MDPI and/or the editor(s) disclaim responsibility for any injury to people or property resulting from any ideas, methods, instructions or products referred to in the content.